

Univerza
v Ljubljani
Fakulteta
za gradbeništvo
in geodezijo



Jamova cesta 2
1000 Ljubljana, Slovenija
<http://www3.fgg.uni-lj.si/>

DRUGG – Digitalni repozitorij UL FGG
<http://drugg.fgg.uni-lj.si/>

Ta članek je avtorjeva zadnja recenzirana različica, kot je bila sprejeta po opravljeni recenziji.

Prosimo, da se pri navajanju sklicujete na bibliografske podatke, kot je navedeno:

University
of Ljubljana
Faculty of
Civil and Geodetic
Engineering



Jamova cesta 2
SI – 1000 Ljubljana, Slovenia
<http://www3.fgg.uni-lj.si/en/>

DRUGG – The Digital Repository
<http://drugg.fgg.uni-lj.si/>

This version of the article is author's manuscript as accepted for publishing after the review process.

When citing, please refer to the publisher's bibliographic information as follows:

Saje, M., Zupan, D. 2006. The rattling of Euler's disk. *Multidiscipline modeling in materials and structures* 2,1: 49-66. DOI: 10.1163/157361106775249952.

The Rattling of Euler's Disk

M. Saje and D. Zupan

*University of Ljubljana, Faculty of Civil and Geodetic Engineering, Jamova 2,
SI-1115 Ljubljana, Slovenia*

Corresponding author:

M. Saje, University of Ljubljana, Faculty of Civil and Geodetic Engineering,
Jamova 2, SI-1115 Ljubljana, Slovenia, e-mail: msaje@fgg.uni-lj.si

Abstract

The motion of a disk spinning on a horizontal surface has drawn a great deal of interest recently. The objectives of the researches are to find out what produces an increasing rattling sound and why the spinning ends so abruptly. In order to understand the behaviour of the spinning disk better, we derived a mathematical model of the rolling/sliding motion of a thin, rigid disk on a rigid, rough horizontal plane, and found the numerical solution of the related initial value problem. Then we studied the motion of the commercially available Tangent Toy disk [3]. The results show that the normal contact force becomes very large whenever the inclination of the disk becomes small. As the inclination of the disk oscillates with time, the time-graph of the normal contact force exhibits periodical peaks, which correlate well with the peaks in the recorded sound response. They could well be responsible for the rattling sound heard during the motion.

Keywords

Euler's disk, Rolling, Sliding, Numerical solution, Rattling sound.

1 Introduction

The motion of a rigid disk on a rough horizontal plane, a typical example of which is a science toy called “Euler’s disk” [3], has been arousing a considerable interest since Moffatt [11] presented his explanation of the settling process of the spinning disk. Moffatt [11] assumed that viscous dissipation in the thin layer of air between the disk and the plane was the reason for the observed abruptness of the settling and the finite-time singularity of the angular velocity. His conclusions were supported neither by experiments performed by Caps *et al.* [4], Easwar *et al.* [5] and van den Engh *et al.* [6], nor by theoretical-experimental results by McDonald and McDonald [10]. Ruina [12] argued that, in many cases, the sliding friction was more important than the viscous dissipation. Stanislavsky and Weron [14] showed that the cusp catastrophe may occur at a sufficiently small inclination of the disk.

A more comprehensive theoretical model was proposed by Kessler and O’Reilly [8]. They assumed that the disk was a rigid cylindrical body with a sharp edge and a finite thickness. They considered the transitions from rolling to sliding (and *vice versa*) during motion, and accounted for a small deformability of the supporting plane, which resulted in a non-zero frictional moment in addition to the frictional force at the point of contact. The related system of differential-algebraic equations and initial conditions was solved numerically. They made a proposition that the oscillating, and always positive normal contact force excites vibrations in the disk (and in the supporting surface), which produces the sound. They further conjectured that the vibrations would result in the disk losing contact with the surface at a small inclination. The impacts of the disk and the plane that follow will constitute an abrupt end of the motion [8].

A minor refinement of their model was presented by Batista [1,3] who, unlike Kessler and O'Reilly [8], assumed that the edge of the disk was rounded.

In the present paper, we explain what produces the rattling sound during the spinning and the settling of the disk. We derive a similar, yet not fully equal rigid-body model of the motion of the disk. We consider the sliding of the disk and the air resistance, but neglect the deformability of the supporting plane, the frictional moment and the thickness of the disk. In the first part of the paper, we briefly describe the governing equations of the motion of the disk and discuss the conditions for the transition between the rolling and sliding. The essential part of the paper is the presentation and the discussion of the numerical results for the spinning motion of the Tangent Toy Euler's disk [3]. We also present the analytical relations between the normal contact force and the inclination of the disk. These relations show periodic peaks occurring with the frequency which very well correlates with the "rattling" frequency of the recorded sound response of the Tangent Toy Euler's disk [3].

2 Description of the model and the equations of motion

Coordinate systems. We consider the disk to be a rigid, planar, homogeneous, perfect circular body of mass m and radius a with the thickness small enough to be neglected. The geometry of the disk is described in a moving Cartesian coordinate system (x, y, z) with its origin at the center of the mass of the disk, and with the right-handed ortho-normal basis $(\mathbf{e}_x, \mathbf{e}_y, \mathbf{e}_z)$. [Base vector \mathbf{e}_z is perpendicular to the disk during motion; \mathbf{e}_x points to the current contact point between the disk and the horizontal surface, and $\mathbf{e}_y = \mathbf{e}_z \times \mathbf{e}_x$.] The position of the disk relative to the space is described in a spatial Cartesian

coordinate system (X, Y, Z) with the origin at a point on the horizontal plane, and with the right-handed ortho-normal basis $(\mathbf{E}_X, \mathbf{E}_Y, \mathbf{E}_Z)$. [Base vectors \mathbf{E}_X and \mathbf{E}_Y lie in the plane, and \mathbf{E}_Z is its normal so that $\mathbf{E}_X \times \mathbf{E}_Y = \mathbf{E}_Z$]. The relation between the two bases is described by the first two of the 3–2–3 Euler angles, precession ψ and nutation ϑ [7].

Kinematics. The components of the angular velocity vector of the moving frame, $\boldsymbol{\omega}$, and of the disk, $\boldsymbol{\Omega}$, both with respect to the moving basis, are

$$\omega_x = -\dot{\psi} \sin \vartheta, \quad \omega_y = \dot{\vartheta}, \quad \omega_z = \dot{\psi} \cos \vartheta, \quad (1)$$

$$\Omega_x = \omega_x, \quad \Omega_y = \omega_y, \quad \Omega_z = \omega_z + \dot{\varphi}. \quad (2)$$

Rotation φ is the third of the 3–2–3 Euler angles.

The position of the disk and its particles in space is fully determined by the position vector of the center of the mass of the disk

$$\mathbf{r} = X\mathbf{E}_X + Y\mathbf{E}_Y + Z\mathbf{E}_Z, \quad (3)$$

and by the rotation of the body, identified by angles ψ, ϑ, φ . However, not all of the six coordinates, $X, Y, Z, \psi, \vartheta, \varphi$, are independent, because the disk is constrained to roll or slide on the plane.

We assume that the disk and the plane are in a single-point contact. Let the material point (a ‘particle’ of the disk), currently in contact with the plane, be denoted by C, its position vector relative to the center of the mass by $\boldsymbol{\rho}_C = a\mathbf{e}_x$, and its velocity vector by \mathbf{v}_C . As material point C must remain on the plane, its velocity vector is the planar vector

$$\mathbf{v}_C = v_C \mathbf{e}_s = v_C \cos \beta \mathbf{E}_X + v_C \sin \beta \mathbf{E}_Y. \quad (4)$$

The velocity vector is described by the slip speed of the contact material

point, $v_C \in (-\infty, \infty)$, and by the slip direction, \mathbf{e}_s , uniquely described by its inclination angle, $\beta \in [0, 2\pi]$, with respect to axis \mathbf{E}_X . If the disk is rolling, $\mathbf{v}_C = \mathbf{0}$; consequently, $v_C = 0$, while β does not have sense.

Since the disk is assumed to be rigid, the velocity of the contact material point is related to the velocity of the center of the mass, \mathbf{v} , and the angular velocity vector of the disk, $\boldsymbol{\Omega}$, by the equation

$$\mathbf{v}_C = \mathbf{v} + \boldsymbol{\Omega} \times a\mathbf{e}_x. \quad (5)$$

In the sliding case, we will employ the contact point velocity vector and not the velocity of the mass center as the basic unknown. In this case

$$\mathbf{v} = \mathbf{v}_C - \boldsymbol{\Omega} \times a\mathbf{e}_x \quad (6)$$

will be substituted with \mathbf{v}_C and $\boldsymbol{\Omega}$ whenever \mathbf{v} will be needed in the derivation of the equations of motion.

Forces. We consider three external forces on an isolated disk: the vertical gravitational force, $\mathbf{F}_g = -mg\mathbf{E}_Z$; the reactive force at the point of contact, \mathbf{R}_C ; and the air resistance over the side surfaces of the disk which results in point force and moment vectors at the center of the disk, \mathbf{F}_a and \mathbf{M}_a .

Force \mathbf{R}_C at the contact has two vector components: the normal force $\mathbf{N} = N\mathbf{E}_Z$ ($N \geq 0$), and the frictional force \mathbf{T} . In the sliding case, the frictional force acts opposite to the sliding, i.e.

$$\mathbf{T} = -T\mathbf{e}_s = R_X\mathbf{E}_X + R_Y\mathbf{E}_Y = T \cos \alpha \mathbf{E}_X + T \sin \alpha \mathbf{E}_Y, \quad T \geq 0, \quad (7)$$

where

$$\alpha = \beta - \pi \in [0, 2\pi]. \quad (8)$$

The two force components, $T \geq 0$ and $N \geq 0$, are assumed to be related by the Coulomb law which says that during sliding their ratio is equal to the dynamic coefficient of friction, $\mu_d \geq 0$:

$$T = \mu_d N. \quad (9)$$

In the rolling case, T is not directly related to N . It must be small enough, though, to prevent the slip, i.e., it must satisfy the inequality

$$T < \mu_{st} N. \quad (10)$$

Here $\mu_{st} \geq \mu_d$ is the static coefficient of friction. Both dynamic and static coefficients of friction are assumed to be constant during the motion.

We assume that the surface traction due to the air resistance, \mathbf{p}_a , acts at each material point of the disk surface in the opposite direction of its velocity vector relative to the air, with the intensity which is linearly proportional to the relative normal velocity of the air. That is,

$$\mathbf{p}_a = -\mu_a(v_z - w_z)\mathbf{e}_z. \quad (11)$$

The difference $v_z - w_z$ is the z -component of the relative velocity of the material point of the disk with respect to the moving air. Parameter $\mu_a \geq 0$ denotes the air resistance coefficient. The resultant point force and moment vectors with respect to the center of the disk are obtained by the integration of traction (11) over the lateral surfaces of the disk.

Equations of motion. The equations of motion of the rigid disk are obtained from the balance of linear momentum, and the balance of angular momentum with respect to the center of mass. In the analysis, the equations of motion are needed in the component form. We express the linear momen-

tum equation with respect to the spatial basis, and the angular momentum equation with respect to the moving basis. The equations of motion must be supplemented by the conditions relating the forces and the velocity of the contact material point, and by the initial conditions. In what follows, we present only a brief review of the equations. The details of the derivation are presented in [13]. For convenience, we consider the rolling and the sliding cases separately.

■ *Equations of the motion of the rolling disk.* Equations of the rolling motion constitute a system of differential–algebraic equations in which only contact force \mathbf{R}_C appears algebraically. Because non-linear DAE equations often cause inconveniences if tackled numerically, we express \mathbf{R}_C from the linear momentum equation with the remaining unknowns and insert it into the angular momentum equation. This way we obtain three scalar first-order differential equations. When complemented with the angle–angular velocity relations (1) and (2), with the no-sliding conditions in the differential form ($\dot{V}_{CX} = \dot{V}_{CY} = \dot{V}_{CZ} = 0$), and with the differential equations relating the position vector of the mass center and its velocity vector ($V_X = \dot{X}$, $V_Y = \dot{Y}$, $V_Z = \dot{Z}$), we obtain 12 first-order differential equations for 12 unknowns $X, Y, Z, V_X, V_Y, V_Z, \psi, \vartheta, \varphi, \Omega_x, \Omega_y$ and Ω_z . The complete set of differential equations along with the related set of initial conditions is displayed in Boxes 1 and 2. Box 1 also provides the formulae for the determination of the secondary variables, i.e. contact forces R_X, R_Y, N, T and angle α . The existence and the uniqueness of the solution of this initial value problem are guaranteed whenever $\vartheta \in (0, \pi)$ [13].

■ *Equations of the motion of the sliding disk.* When the disk slides, the equations of motion are reformulated in the following manner: in the first

step, we substitute the components of the velocity vector of the center of mass, V_X and V_Y , with v_C and α by using equations (6), (4) and (8). In the second step, we substitute R_X and R_Y with T and α , using equation (7). In the last step, after inserting equation (9), we eliminate T and N . After adding the angle–angular velocity relations (1) and (2), the contact condition $V_{CZ} = 0$ in the differential form ($\dot{V}_{CZ} = 0$), and the differential equation which relates the position vector (3) of the center and its velocity vector, we have 12 first-order differential equations for 12 unknowns $X, Y, Z, v_C, \alpha, V_Z, \psi, \vartheta, \varphi, \Omega_x, \Omega_y$ and Ω_z . The complete set of differential equations along with the initial conditions is displayed in Boxes 3 and 4.

This time the existence and the uniqueness of the solution of the initial value problem for the sliding are not automatically assured for all $\vartheta \in (0, \pi)$, the exceptions being $\vartheta = 0, \vartheta = \pi, v_C = 0$ and $A + ma^2 \cos \vartheta \left[\mu_d \cos(\alpha - \psi) \sin \vartheta + \cos \vartheta \right] = 0$ [13].

■ *Rolling-to-sliding and sliding-to-rolling transitions.* As $\nu = T/N$ generally varies with time during the rolling, it may become equal to μ_{st} at a particular instant. The sliding then begins, and the governing equations of Box 1 must be replaced by the equations in Box 3. The initial values of variables for the sliding motion to follow, i.e. $X_0, Y_0, Z_0, v_C^0 = 0, V_Z^0, \psi_0, \vartheta_0, \varphi_0, \Omega_x^0, \Omega_y^0, \Omega_z^0$, are the current values of these variables at the end of the rolling motion. Note that when the dynamic and static friction coefficients are different (which is often the case), the frictional force T suffers a discontinuity jump.

During the sliding motion, the slip speed changes with time. At a particular time it may vanish. Which kind of the motion follows, depends on the ratio of contact forces, T_r/N_r , determined from the current values of variables from

the equations of the motion for the rolling disk (see Box 1):

$$T_r = \sqrt{(R_X^r)^2 + (R_Y^r)^2}, \quad N_r = R_Z^r = m(\dot{V}_Z + g) + \mu_a \pi a^2 (v_z - w_z) \cos \vartheta. \quad (12)$$

The time derivatives \dot{V}_X , \dot{V}_Y and \dot{V}_Z , required in equations (12), are obtained from the equations of the motion for the rolling disk, using current values of variables. There are two possibilities:

(i) End of sliding. If $T_r/N_r < \mu_{st}$, the disk “sticks” and the motion which follows is the rolling, so the equations in Boxes 3 and 4 are replaced by the equations from Boxes 1 and 2.

(ii) Sliding continues. If $T_r/N_r \geq \mu_{st}$, the disk will continue to slide, and the equations from Boxes 3 and 4 remain valid.

At the end of each time-integration step, we have to examine the slip speed, the static friction criterion as discussed above, and the normal contact force condition ($N \geq 0$) to find out if any of the criteria is violated. If so, then some transition takes place, and we must determine the time of transition, calculate the current values of variables, and use them as the initial values in the appropriate system of differential equations, Box 1 or Box 3. If N becomes negative, the disk loses contact with the plane. As the free flight and the subsequent impact of the disk onto the plane are not dealt with here, the integration stops.

3 Results

The equations of the motion of the disk, supplemented by the initial and the transition conditions, constitute an initial value problem. We solve it numer-

ically by the help of computer program **Matlab** [9]. The program employs various Runge–Kutta methods and offers a number of solution functions, of which we choose functions **ode45** and **ode15s**. The local relative and absolute integration errors are chosen to be $\text{RelTol}=10^{-8}$ and $\text{AbsTol}=10^{-10}$, respectively. The global error cannot be controlled directly. Critical events, such as the transition from rolling to sliding, or the loss of contact, are detected within the machine precision (approximately 10^{-16}) by the **Matlab** function **Events**.

We assume that the disk has the same dimensions as the Tangent Toy Euler’s disk [3], i.e. $a = 3.755$ cm, $m = 0.4387$ kg. In the analysis we disregard the thickness of the disk.

The dynamic coefficient of friction was chosen to be $\mu_d = 0.115$, as obtained in the friction coefficient measurements performed on the Tangent Toy disk [2]. The static coefficient of friction was assumed to be somewhat bigger ($\mu_{st} = 0.2$). These are generally small, yet realistic values for the Tangent Toy disk.

As in [8] we take that the disk is initially inclined to the horizontal plane and given an initial angular velocity about \mathbf{e}_x . The corresponding initial conditions are:

$$\begin{aligned} X_0 &= 0, & Y_0 &= 0, & Z_0 &= a \sin \vartheta_0, \\ V_X^0 &= 0, & V_Y^0 &= 0, & V_Z^0 &= 0, \\ \psi_0 &= 0, & \vartheta_0 &= \frac{\pi}{2} - 1, & \varphi_0 &= 0, \\ \Omega_x^0 &= 1, & \Omega_y^0 &= 0, & \Omega_z^0 &= 0. \end{aligned}$$

First we assess the effect of the air resistance on the motion. Numerical experiments show that the linear air resistance model as assumed here has a negligible influence on the motion of the Tangent Toy Euler’s disk.

The numerical solution shows that the disk starts sliding at the very beginning of the motion. During the subsequent motion, the inclination of the disk, ϑ , oscillates with time as shown in Figure 1a for the first second of the motion, and in Figure 1b for the 99th second of the motion. Figure 2 shows the envelopes of maximal and minimal amplitudes of ϑ for the first 100-second time interval of motion. We observe that the maximal amplitude of the inclination angle decreases all the time but remains nearly constant (0.05 rad) during the second part of the motion. This corresponds to the actual behaviour of the Tangent Toy Euler's disk.

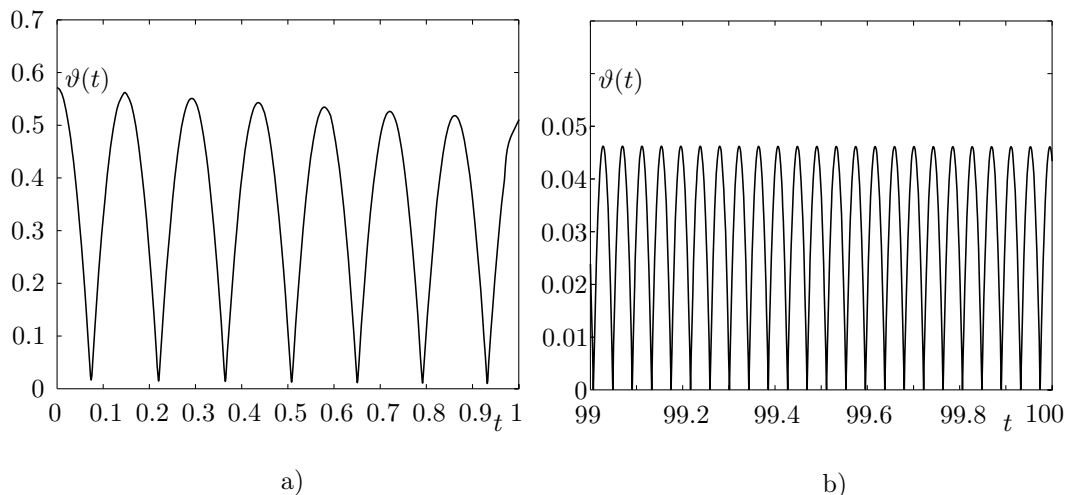


Fig. 1. The variation of ϑ with time; (a) in interval $[0, 1]$ s; (b) in interval $[99, 100]$ s.

Figure 3 shows the related graphs of the time derivative of the inclination, $\dot{\vartheta}$. It is clear from these graphs that $\dot{\vartheta}$ is not a slowly varying function of time. This quantity is not small compared to $\dot{\psi}$ either (see Figure 4), as assumed by Moffatt [11] and Stanislavsky and Weron [14] in their theoretical derivations of the finite-time settling of the disk.

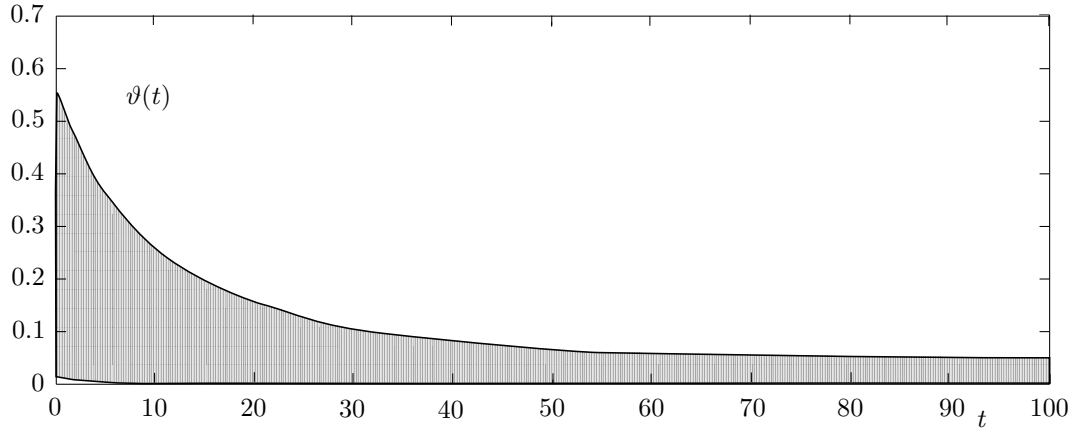


Fig. 2. Envelopes of maximal and minimal amplitudes of ϑ in interval $[0, 100]$ s.

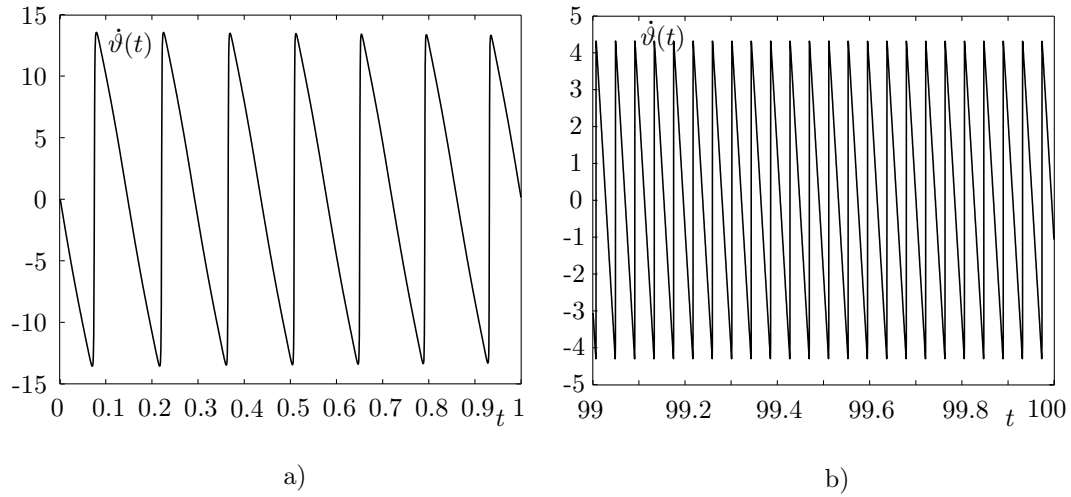


Fig. 3. The variation of $\dot{\vartheta}$ with time; (a) in interval $[0, 1]$ s; (b) in interval $[99, 100]$ s.

The variations of ν with time are depicted in Figure 5. The figure shows that the sliding is almost regularly interrupted by a short interval of the rolling. We can observe abrupt changes of ν from 0.115 to 0.2 (and *vice versa*), which is due to the difference between the static and dynamic coefficients of friction.

The variation of the slip speed is displayed in Figure 6 for short intervals of time ($[0, 1]$ s and $[99, 100]$ s), and in Figure 7, in the form of the envelope of the maximal amplitude of v_C in the time interval $[0, 100]$ s. We see that the

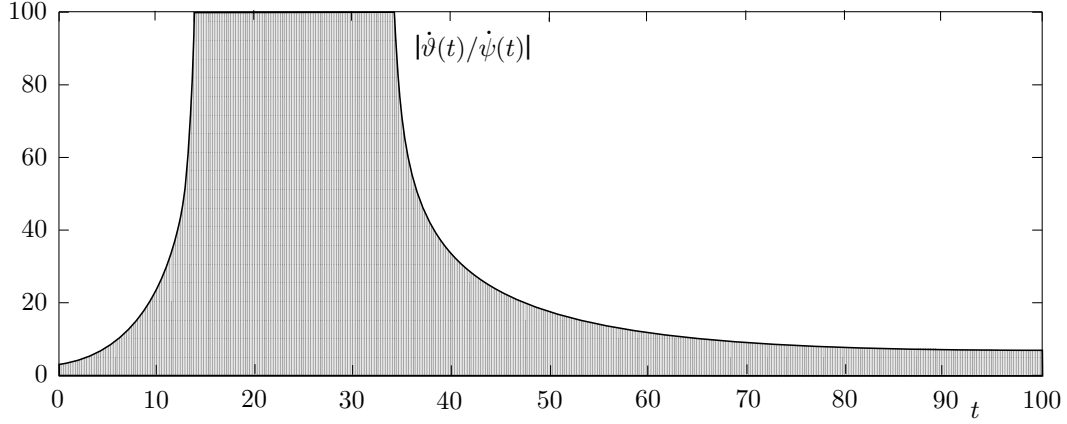


Fig. 4. The variation of $\left| \frac{\dot{\vartheta}}{\dot{\psi}} \right|$ with time in interval $[1, 100]$ s.

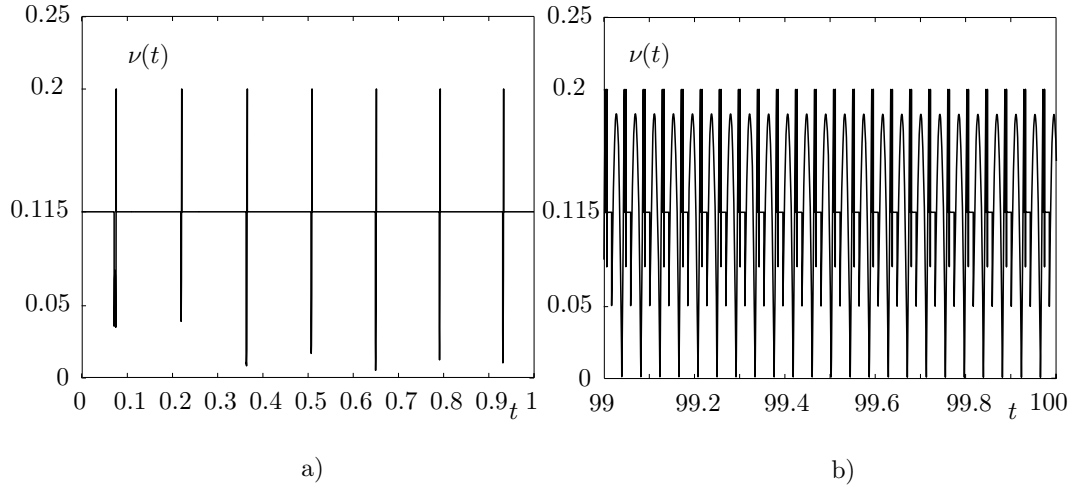


Fig. 5. The variation of ν with time; (a) in interval $[0, 1]$ s; (b) in interval $[99, 100]$ s.

slip speed wildly oscillates during the motion. At instants when $v_C = 0$, the rolling takes place. The rolling motion appears rather regularly, particularly in the settling phase (Figure 6b), in which the dominating rolling motion is interrupted by the short sliding motion roughly 24-times per second. Once the maximal inclination angle of the disk becomes small (at about 50 s, its value is roughly 0.05 rad), the maximal slip speed also becomes small (at most about $8 \cdot 10^{-4}$ m/s), but it is still non-zero and remains such, because the static coefficient of friction is so small. This kind of behaviour will in our model

continue for $t > 100$ s, i.e. the disk will never start a pure rolling motion.

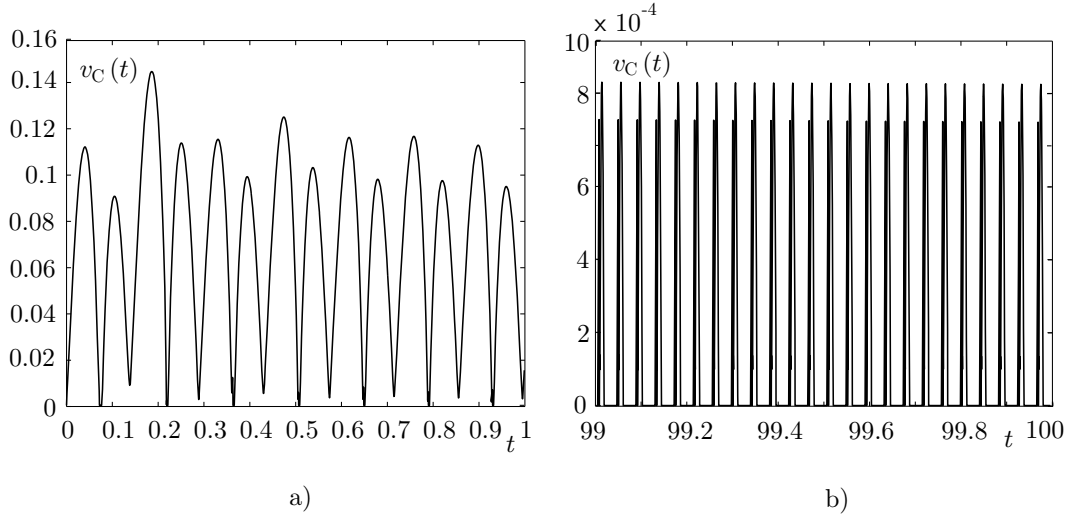


Fig. 6. The variation of v_C with time; (a) in interval $[0, 1]$ s; (b) in interval $[99, 100]$ s.

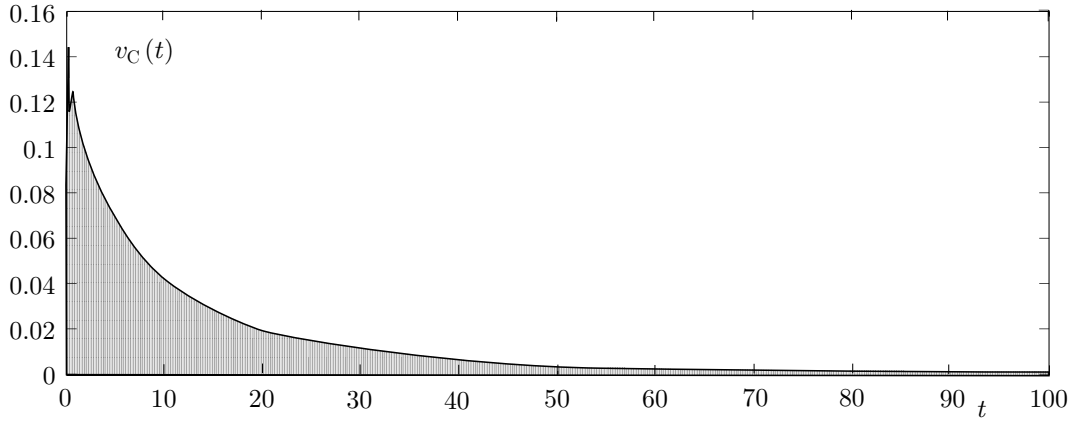


Fig. 7. Envelopes of maximal amplitudes of v_C in interval $[0, 100]$ s.

The variation of the reduced normal contact force, N/mg , with time is displayed in Figure 8 for intervals $[0, 1]$ s and $[99, 100]$ s. For comparison reasons, the figure also displays the graph of the inclination of the disk, ϑ . Note that the normal contact force, N , and the inclination, ϑ , have the same frequency of oscillations, with the period and the frequency being initially 0.14 s and 44 s^{-1} ,

respectively (Figure 8a) in the interval $[0, 1]$ s, and 0.042 s and 149 s^{-1} , respectively, in the interval $[99, 100]$ s (Figure 8b). Observe also that N is large when ϑ is small, and *vice versa*. The comparison between Figures 8 and 5 shows that the rapid increase and the subsequent rapid decrease of the normal contact force take place always during rolling phases. From Figure 8 you may see that the normal force is positive at all times, which indicates that the disk does not lose contact with the surface. The relation between the normal contact force and the inclination angle is a complicated function. The graph of its envelope is a snail-shaped curve depicted in Figure 9.

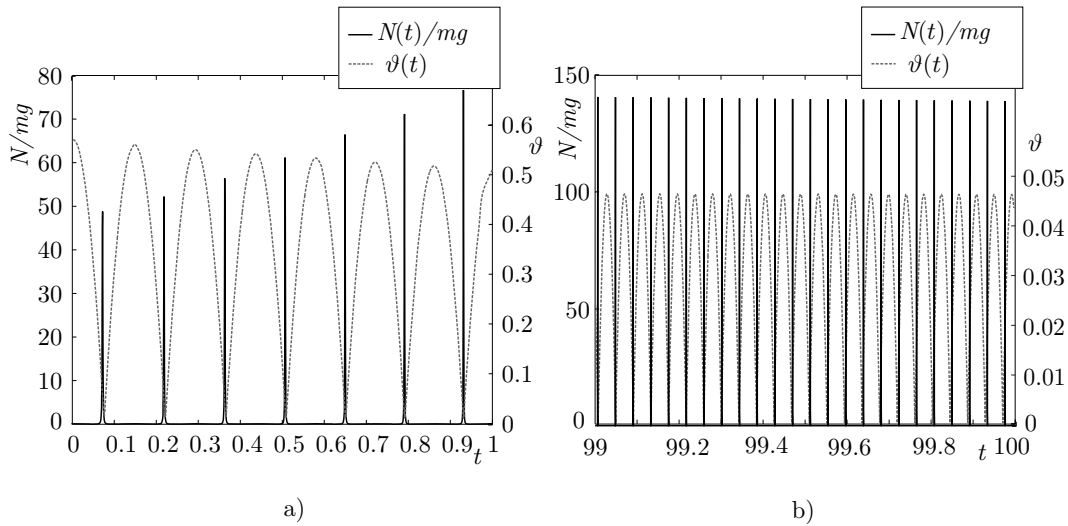


Fig. 8. The variation of N/mg and ϑ with time; (a) in interval $[0, 1]$ s; (b) in interval $[99, 100]$ s.

Figure 8 reveals an interesting phenomenon of the rolling and sliding disk, i.e. a periodical appearance of high peaks of the normal contact force at small inclination angles (see the dotted lines in Figure 8). These peaks are not the consequence of the error of the numerical solution, because they can be confirmed by the analytical solution for N in terms of ϑ , Ω_x , Ω_y and Ω_z . This

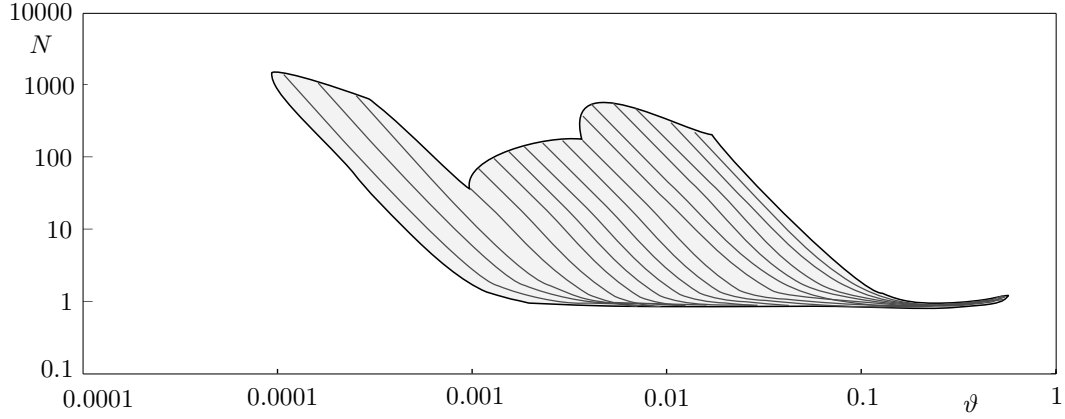


Fig. 9. The envelope of N vs ϑ in interval $[1, 100]$ s.

is easily obtained by the elimination of time derivative \dot{V}_Z from $N = m(\dot{V}_Z + g)$ using the equations of the motion given in Boxes 1 and 3 (while neglecting the air resistance). For the rolling motion, the analytical solution gives:

$$\frac{N}{mg} = \alpha_1 + \frac{\alpha_2}{\sin \vartheta}, \quad (13)$$

where α_1 and α_2 denote

$$\begin{aligned} \alpha_1 &= \frac{a \cos \vartheta}{g(ma^2 + A)} \left[(C + ma^2)\Omega_x\Omega_z - mga \cos \vartheta \right] - \frac{a\Omega_y^2 \sin \vartheta}{g} + 1, \\ \alpha_2 &= \frac{aA\Omega_x^2}{g(ma^2 + A)} \cos^2 \vartheta. \end{aligned} \quad (14)$$

[A and C are the moments of inertia about the axes y and z of the disk (see Box 1).] α_1 and α_2 are finite for any ϑ and any finite angular velocities Ω_x , Ω_y and Ω_z . In contrast, the normal contact force grows towards infinity when ϑ approaches 0 or π . For a given α_1 and α_2 , but with ϑ approaching 0 (or π), the graph N vs ϑ of (13) exhibits the peak whose shape completely agrees with the one found numerically (see Figure 8). In short, equation (13) clearly shows that the amplitude of the normal contact force largely depends on the current inclination, ϑ , of the disk, and tends to infinity when ϑ goes to 0 or π . As α_2 is proportional to Ω_x^2 , the normal contact force does not exhibit the

peak if $\Omega_x = 0$ at $\vartheta = \vartheta_{\min}$.

For the sliding motion, the analytical solution gives:

$$\frac{N}{mg} = \alpha_3 + \frac{\alpha_4}{\sin \vartheta}, \quad (15)$$

where α_3 and α_4 are given by

$$\alpha_3 = \frac{A}{\beta_0} \left[1 - \frac{a\Omega_y^2}{g} \sin \vartheta \right] + \frac{aC\Omega_x\Omega_z}{g\beta_0} \cos \vartheta, \quad \alpha_4 = \frac{aA\Omega_x^2}{g\beta_0} \cos^2 \vartheta \quad (16)$$

with β_0 being an auxiliary variable

$$\beta_0 = ma^2 \cos \vartheta [\mu_d \cos(\alpha - \psi) \sin \vartheta + \cos \vartheta] + A.$$

As in the rolling case, α_3 and α_4 are finite for any ϑ and finite angular velocities. The numerical test shows that β_0 is not equal to zero during the motions studied here. Therefore, the normal contact force grows towards infinity when ϑ approaches 0 or π . The shape of the graph N vs ϑ of the analytical solution (15) fully agrees with the shape of the corresponding graph, obtained numerically. This confirms our surprising numerical results. We stress again that not all of the peaks of the normal contact force, yet a great majority of them, take place during rolling phases.

The results show that the rigid-body model suffers a sequence of ‘shocks’ of very short-lasting normal contact forces of very large amplitudes. These large values probably stem from the assumption that the supporting plane and the disk are rigid. For a deformable supporting plane and/or disk, the amplitudes of the normal contact forces would probably be smaller, but we believe that the time-graph of N would still exhibit peaks.

Such a series of ‘impact’ forces could well be responsible for sounds heard during the motion. In order to verify the assumption, we compare a recorded

sound vs time graph [3] of the spinning Tangent Toy disk with the calculated N/mg vs time graph in Figure 10. We display the recorded graph of a one second interval approximately 4 to 5 seconds before the disk stops. The calculated graph is displayed for the interval [99, 100] s. Figure 10 clearly shows that the frequencies of the recorded sound and the normal contact force peaks are nearly equal, the frequency of the sound peaks being 154 s^{-1} and that of the calculated 149 s^{-1} .

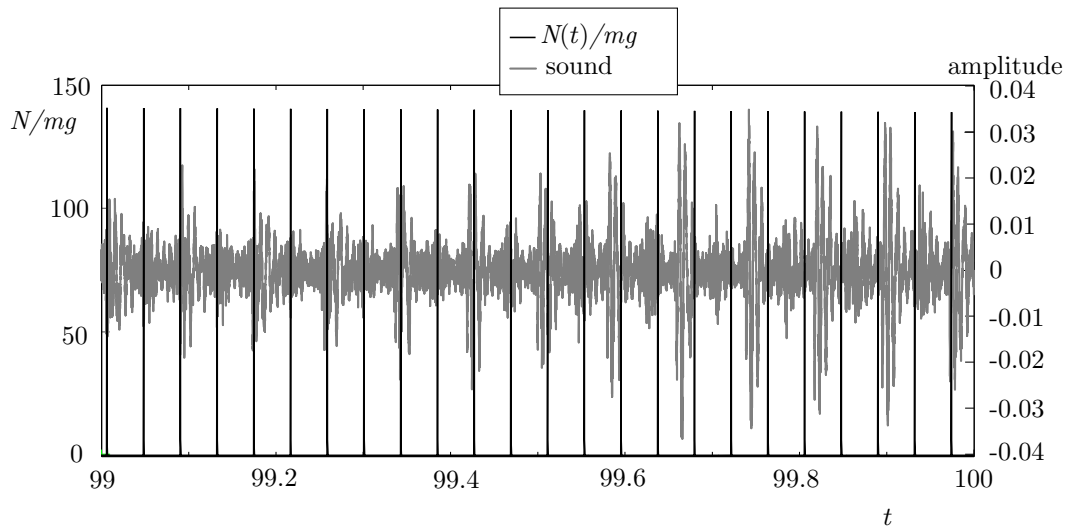


Fig. 10. The comparison between the recorded sound and the calculated normal contact force time-graphs during the ending phase of the motion.

Such a periodic highly-localized kind of time variation of the normal contact force is different from that presented by Kessler and O'Reilly [8] for a thick disk. This may indicate that the thickness of the disk has an important effect on its motion.

4 Conclusions

We applied the equations of the motion of a thin rigid disk and assumed a rigid supporting plane to describe the rolling–sliding motion of the Tangent Toy Euler’s disk [3]. We assumed realistic, but different values of the dynamic and static coefficients of friction and the linear air resistance law. Our numerical and partly analytical results show (i) that the normal contact force is positive all the time, so that the disk does not lose the contact during its motion, and (ii) that the normal contact force becomes very large whenever the inclination of the disk becomes small. Consequently, the time-graph of the normal contact force exhibits impact-like peaks with the frequency from about 44 s^{-1} during the initial stages, to 149 s^{-1} at about 100 s. The comparison of two graphs, the time graph of the recorded sound of the Tangent Toy disk and the time graph of the normal contact force, in one-second time interval about 4 to 5 seconds before the disk stops, shows a very good correlation between the sound and the force peaks. Thus, the series of ‘impact-like forces’ seems to be responsible for the rattling heard during the motion of the disk.

References

- [1] M. Batista, Proceeding of the Slovenian Society of Mechanics, Kuhelj’s days 2004, September 30–October 1, 2004, 9–16 (2004).
- [2] M. Batista, Private communication (2004).
- [3] J. Bendik, The official Euler’s disk website, <http://www.eulerdisk.com>, Tangent Toy Co., Sausalito, CA, <http://www.tangenttoy.com>.
- [4] H. Caps, S. Dorbolo, S. Ponte, H. Croisier, N. Vandewalle, Condensed Matter,

0401278 v1, January 16 (2004).

- [5] K. Easwar, F. Rouyer, N. Menon, Physical Review E **66** 045102(R) (2002).
- [6] G. van den Engh, P. Nelson, J. Roach, Nature **404**, 540 (2000).
- [7] H. Goldstein, Classical mechanics, 2nd edition, Addison-Wesley, Reading (1981).
- [8] P. Kessler, O. M. O'Reilly, Regular and Chaotic dynamics **7**, (1) 49–60 (2002).
- [9] The MathWorks, Inc., *MATLAB, Using MATLAB*, Natick, <http://www.mathworks.com> (1999).
- [10] A. J. McDonald, K. T. McDonald, Preprint Archive, Los Alamos National Laboratory, arXiv: physics/008227, 20 p (2000).
- [11] H. K. Moffatt, Nature **404**, 833–834 (2000).
- [12] A. Ruina, Comments on “Euler’s disk and its finite-time singularity by H. K. Moffatt”, unpublished notes, Dept. of Theoretical and Appl. Mechanics, Cornell University, 7 p (2000).
- [13] M. Saje, D. Zupan, Motion of a disk on a rough horizontal surface, The official Kinematics and dynamics website for students, University of Ljubljana, Faculty of Civil and Geodetic Engineering, <http://www.km.fgg.uni-lj.si>.
- [14] A. A. Stanislavsky, K. Weron, Physica D **156**, 247–259 (2001).

Box 1. Rolling. Differential equations of motion

Primary unknowns: $X, Y, Z, V_X, V_Y, V_Z, \psi, \vartheta, \varphi, \Omega_x, \Omega_y, \Omega_z$

$$(1) \quad \dot{X} = V_X$$

$$(2) \quad \dot{Y} = V_Y$$

$$(3) \quad \dot{Z} = V_Z$$

$$(4) \quad A\Omega_y\dot{\varphi} + A\dot{\Omega}_x = (A - C)\Omega_y\Omega_z - \frac{1}{4}\mu_a\pi a^4\Omega_x$$

$$(5) \quad (ma \cos \psi \sin \vartheta) \dot{V}_X + (ma \sin \psi \sin \vartheta) \dot{V}_Y + (ma \cos \vartheta) \dot{V}_Z \\ - A\Omega_x\dot{\varphi} + A\dot{\Omega}_y \\ = (C - A)\Omega_x\Omega_z - mga \cos \vartheta - \frac{1}{4}\mu_a\pi a^4\Omega_y - \mu_a\pi a^3(v_z - w_z)$$

$$(6) \quad (ma \sin \psi) \dot{V}_X - (ma \cos \psi) \dot{V}_Y + C\dot{\Omega}_z = 0$$

$$(7) \quad \sin \vartheta \dot{\psi} = -\Omega_x$$

$$(8) \quad \dot{\vartheta} = \Omega_y$$

$$(9) \quad \cos \vartheta \dot{\psi} + \dot{\varphi} = \Omega_z$$

$$(10) \quad \dot{V}_X - a \left[(-\Omega_y \sin \psi \sin \vartheta + \Omega_z \cos \psi) \dot{\psi} + \Omega_y \cos \psi \cos \vartheta \dot{\vartheta} \right. \\ \left. + \cos \psi \sin \vartheta \dot{\Omega}_y + \sin \psi \dot{\Omega}_z \right] = 0$$

$$(11) \quad \dot{V}_Y + a \left[-(\Omega_y \cos \psi \sin \vartheta + \Omega_z \sin \psi) \dot{\psi} - \Omega_y \sin \psi \cos \vartheta \dot{\vartheta} \right. \\ \left. - \sin \psi \sin \vartheta \dot{\Omega}_y + \cos \psi \dot{\Omega}_z \right] = 0$$

$$(12) \quad \dot{V}_Z + a(\Omega_y \sin \vartheta \dot{\vartheta} - \cos \vartheta \dot{\Omega}_y) = 0$$

Secondary unknowns: R_X, R_Y, T, N, α

$$R_X = m\dot{V}_X + \mu_a\pi a^2(v_z - w_z) \cos \psi \sin \vartheta$$

$$R_Y = m\dot{V}_Y + \mu_a\pi a^2(v_z - w_z) \sin \psi \sin \vartheta$$

$$T = \sqrt{R_X^2 + R_Y^2}, \quad N = R_Z = m(\dot{V}_Z + g) + \mu_a\pi a^2(v_z - w_z) \cos \vartheta$$

$$\sin \alpha = R_Y/T, \quad \cos \alpha = R_X/T \Rightarrow \alpha \in [0, 2\pi]$$

$$A = \frac{1}{4}ma^2, \quad C = \frac{1}{2}ma^2$$

Box 2. Rolling. Initial conditions

Initial conditions		
$X(t_0) = X_0,$	$Y(t_0) = Y_0,$	$Z(t_0) = Z_0$
$V_X(t_0) = V_X^0,$	$V_Y(t_0) = V_Y^0,$	$V_Z(t_0) = V_Z^0$
$\psi(t_0) = \psi_0,$	$\vartheta(t_0) = \vartheta_0,$	$\varphi(t_0) = \varphi_0$
$\Omega_x(t_0) = \Omega_x^0,$	$\Omega_y(t_0) = \Omega_y^0,$	$\Omega_z(t_0) = \Omega_z^0$
Constraints		
$V_X^0 - a(\Omega_y^0 \cos \psi_0 \sin \vartheta_0 + \Omega_z^0 \sin \psi_0) = 0$		
$V_Y^0 + a(-\Omega_y^0 \sin \psi_0 \sin \vartheta_0 + \Omega_z^0 \cos \psi_0) = 0$		
$V_Z^0 - a\Omega_y^0 \cos \vartheta_0 = 0$		
$Z_0 - a \sin \vartheta_0 = 0$		

Box 3. Sliding. Differential equations of motion

Primary unknowns: $X, Y, Z, v_C, \alpha, V_Z, \psi, \vartheta, \varphi, \Omega_x, \Omega_y, \Omega_z$

- (1) $\dot{X} = -v_C \cos \alpha + a(\Omega_y \cos \psi \sin \vartheta + \Omega_z \sin \psi)$
- (2) $\dot{Y} = -v_C \sin \alpha + a(\Omega_y \sin \psi \sin \vartheta - \Omega_z \cos \psi)$
- (3) $\dot{Z} = V_Z$
- (4) $mv_C \dot{\alpha} + ma \left[-\Omega_y \cos(\alpha - \psi) \sin \vartheta + \Omega_z \sin(\alpha - \psi) \right] \dot{\psi}$
 $+ ma \Omega_y \sin(\alpha - \psi) \cos \vartheta \dot{\vartheta} + ma \sin(\alpha - \psi) \sin \vartheta \dot{\Omega}_y$
 $+ ma \cos(\alpha - \psi) \dot{\Omega}_z = -\mu_a \pi a^2 (v_z - w_z) \sin(\alpha - \psi) \sin \vartheta$
- (5) $-m\dot{v}_C - \mu_d m \dot{V}_Z + ma \left[\Omega_y \sin(\alpha - \psi) \sin \vartheta + \Omega_z \cos(\alpha - \psi) \right] \dot{\psi}$
 $+ ma \Omega_y \cos(\alpha - \psi) \cos \vartheta \dot{\vartheta} + ma \cos(\alpha - \psi) \sin \vartheta \dot{\Omega}_y$
 $- ma \sin(\alpha - \psi) \dot{\Omega}_z = \mu_d mg$
 $+ \mu_a \pi a^2 (v_z - w_z) \left[\mu_d \cos \vartheta - \cos(\alpha - \psi) \sin \vartheta \right]$
- (6) $A \Omega_y \dot{\varphi} + A \dot{\Omega}_x = (A - C) \Omega_y \Omega_z - \frac{1}{4} \mu_a \pi a^4 \Omega_x$
- (7) $ma \left[\mu_d \cos(\alpha - \psi) \sin \vartheta + \cos \vartheta \right] \dot{V}_Z - A \Omega_x \dot{\varphi} + A \dot{\Omega}_y =$
 $-\frac{1}{4} \mu_a \pi a^4 \Omega_y$
 $+ (C - A) \Omega_x \Omega_z - mga \left[\mu_d \cos(\alpha - \psi) \sin \vartheta + \cos \vartheta \right]$
 $- \mu_a \pi a^3 (v_z - w_z) \cos \vartheta \left[\mu_d \cos(\alpha - \psi) \sin \vartheta + \cos \vartheta \right]$
- (8) $\mu_d ma \sin(\alpha - \psi) \dot{V}_Z + C \dot{\Omega}_z = \mu_d mga \sin(\alpha - \psi)$
 $+ \mu_d \mu_a \pi a^3 (v_z - w_z) \cos \vartheta \sin(\alpha - \psi)$
- (9) $\sin \vartheta \dot{\psi} = -\Omega_x$
- (10) $\dot{\vartheta} = \Omega_y$
- (11) $\cos \vartheta \dot{\psi} + \dot{\varphi} = \Omega_z$
- (12) $\dot{V}_Z + a \left(\Omega_y \sin \vartheta \dot{\vartheta} - \cos \vartheta \dot{\Omega}_y \right) = 0$

Secondary unknowns: T, N, R_X, R_Y, V_X, V_Y

$$T = \mu_d m (\dot{V}_Z + g) + \mu_d \mu_a \pi a^2 (v_z - w_z) \cos \vartheta$$

$$R_X = T \cos \alpha, \quad R_Y = T \sin \alpha, \quad R_Z = N = T / \mu_d$$

$$V_X = -v_C \cos \alpha + a(\Omega_y \cos \psi \sin \vartheta + \Omega_z \sin \psi)$$

$$V_Y = -v_C \sin \alpha + a(\Omega_y \sin \psi \sin \vartheta - \Omega_z \cos \psi)$$

Box 4. Sliding. Initial conditions

Initial conditions		
$X(t_0) = X_0,$	$Y(t_0) = Y_0,$	$Z(t_0) = Z_0$
$v_C(t_0) = v_C^0,$	$\alpha(t_0) = \alpha_0,$	$V_Z(t_0) = V_Z^0$
$\psi(t_0) = \psi_0,$	$\vartheta(t_0) = \vartheta_0,$	$\varphi(t_0) = \varphi_0$
$\Omega_x(t_0) = \Omega_x^0,$	$\Omega_y(t_0) = \Omega_y^0,$	$\Omega_z(t_0) = \Omega_z^0$
Constraints		
$V_Z^0 - a\Omega_y^0 \cos \vartheta_0 = 0$		
$Z_0 - a \sin \vartheta_0 = 0$		

List of Figures

1	The variation of ϑ with time; (a) in interval $[0, 1]$ s; (b) in interval $[99, 100]$ s.	12
2	Envelopes of maximal and minimal amplitudes of ϑ in interval $[0, 100]$ s.	13
3	The variation of $\dot{\vartheta}$ with time; (a) in interval $[0, 1]$ s; (b) in interval $[99, 100]$ s.	13
4	The variation of $\left \frac{\dot{\vartheta}}{\dot{\psi}}\right $ with time in interval $[1, 100]$ s.	14
5	The variation of ν with time; (a) in interval $[0, 1]$ s; (b) in interval $[99, 100]$ s.	14
6	The variation of v_C with time; (a) in interval $[0, 1]$ s; (b) in interval $[99, 100]$ s.	15
7	Envelopes of maximal amplitudes of v_C in interval $[0, 100]$ s.	15
8	The variation of N/mg and ϑ with time; (a) in interval $[0, 1]$ s; (b) in interval $[99, 100]$ s.	16
9	The envelope of N vs ϑ in interval $[1, 100]$ s.	17
10	The comparison between the recorded sound and the calculated normal contact force time-graphs during the ending phase of the motion.	19